An Enzyme-Based Microfluidic Biofuel Cell

Makoto Togo, Hirokazu Kaji, Takashi Abe, and Matsuhiko Nishizawa*

* Professor

Department of Bioengineering and Robotics, Graduate School of Engineering
E-mail: nishizawa@biomems.mech.tohoku.ac.jp

Abstract

We report the construction of microfluidic biofuel cells connected in series by semiautomatic air valves, in which a lotus leaf-like superhydrophobic structure (a micropillar array) traps air and ionically isolates each biofuel cell aligned within the channel. The micropillar array was prepared by conventional photolithography and reactive ion etching (RIE) techniques, and the structural parameters of the micropillars (size and spacing) were optimized as to obtain the highest degree of hydrophobicity. The superhydrophobic gates that have an array of micropillars (20 μm high, 15 μm in diameter and with a 15 μm spacing) reversibly worked as air-valves especially at lower flow rate. The open-circuit voltage measured at the ends of three aligned biofuel cells was three times larger than that of a single cell using the semiautomatic air valve system.

1. Introduction

Enzymatic biofuel cells have attracted attention as on-demand miniature power sources due to their high reaction selectivity that in principle allows direct utilization of common fuel solutions such as fruit juices and body fluids without purification [1-17]. In addition, the high reaction selectivity of enzymes would also make it possible to design separator-free fuel cells that composed of just a couple of anode and cathode electrodes exposed to solutions containing both fuel and oxidant as illustrated in Fig. 1. Since the fuel fluid is typically aqueous neutral solution, the chemical stability of packaging are not always necessarily considered. Despite these merits, there are some problems that need to be solved. The problematic lower power output has recently been improved rapidly (to several mA cm^{-2}) by using nano-materials (i.e. carbon blacks, carbon nanotubes, carbon aerogels and gold nano-particles) as electrode. For example, we have studied the use of carbon black (ketjen black) electrodes modified with Vitamin K_3 (VK_3)-pendant polymer and an enzyme membrane for glucose oxidation. And the glucose electro-oxidation current has reached as high as 2 mA cm^{-2}. In addition, so far, many research groups have studied microfluidic-type biofuel cell made by conventional microfabrication techniques [7,8, 16-19]. Such the cells were studied not just for miniaturization of the system, but for quantitatively evaluation of their performances under regulated conditions. The output currents of the microfluidic biofuel cells were reported to be improved by suitably designing electrode material [7,18] and electrode arrangement [8,17]. Another remaining problem is stability of the cell. The lifetime of an enzymatic biofuel cell is usually determined by enzyme stability which could be improved by protein engineering and immobilized state of enzymes. In recent days, some researchers suggested that the immobilized enzymes within a microstructure, such as a meso-porous carbon matrix [1] or Nafion membrane [2], showed higher stability. On the other hand, the possible output voltage of a single biofuel cell is determined thermodynamically, and is generally lower than 1 V. Therefore, many applications require cell-stacking (a series connection), which is however often troublesome due to short-circuiting of cells through the ion-conductive fuel solution. The series connection of biofuel cells requires a system for ionic isolation between each cell.

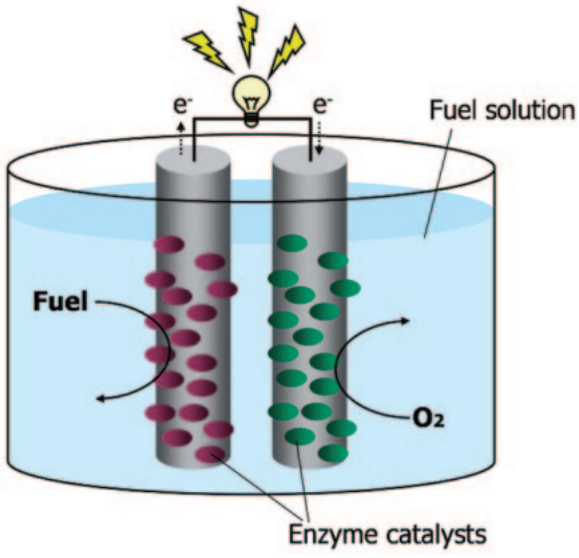

Fig. 1. Illustration of biofuel cell.

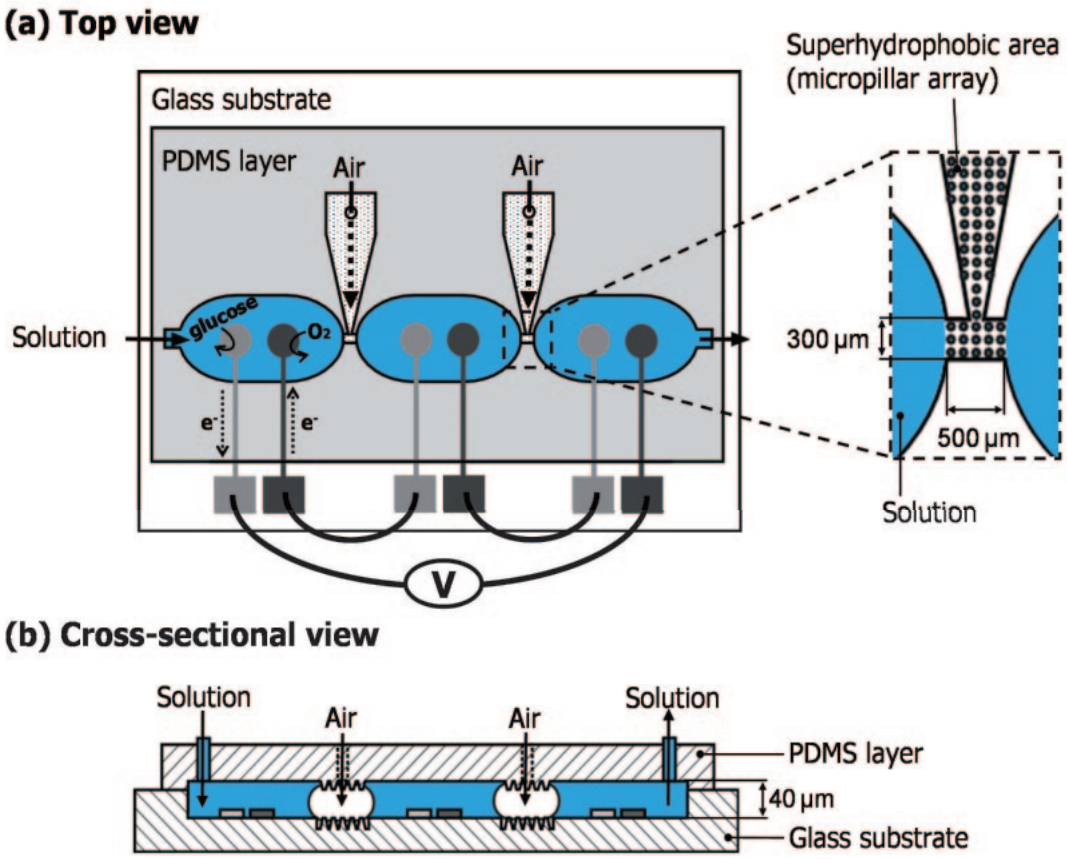

Fig. 2. (a) Top view and (b) cross-sectional view of series-connected biofuel cells on a fluidic chip. Inset shows a close-up top view of the valve area.

In this paper, we have investigated a method to connect microfluidic biofuel cells in series by means of air valves. Our strategy is based on the air-trapping of air at a superhydrophobic area prepared in the fluidic channel in order to ionically isolate as each cell to be ionically isolated. Many researchers have been developed the prepared a superhydrophobic surface by transcribing or mimicking the surface structure of a lotus leaf, which is composed of an array of small hydrophobic small bumps [20-26]. We similarly prepared a lotus leaf-like micropillar array which was designed to be 20 µm in height, 15 µm in diameter, spaced 15 µm apart on the wall of a 40 µm deep microchannel by microfabrication techniques, including reactive ion etching (RIE).

As shown in Fig. 2, three cells are connected by superhydrophobic gates which are 300 µm wide, 500 µm long and 40 µm deep. The bottle-shaped superhydrophobic air reservoirs are open at their ends in order to take in air from the outside. During fuel introduction, all cells are filled with fuel solution, and are isolated each other by air introduced into the superhydrophobic reservoirs. If this automatic air-valve system works as expected, users of this power device never have to introduce fuel solution separately to each chamber. We here report the fabrication procedure for the fluidic devices with the superhydrophobic gates and their basic performance as air-valves for a series-connected biofuel cells.

2. Methods

2.1. Series-connection method

We report the construction of microfluidic biofuel cells connected in series by semiautomatic air valves, in which a lotus leaf-like superhydrophobic structure (a micropillar array) traps air and ionically isolates each biofuel cell aligned within the channel. The micropillar array was prepared by conventional photolithography and reactive ion etching (RIE) techniques, and the structural parameters of the micropillars (size and spacing) were optimized as to obtain the highest degree of hydrophobicity.

2.2. Fabrication of a microfluidic cell

The microfluidic chip containing the hydrophobic valve parts was constructed by binding two components: a glass substrate with electrodes (bottom layer) and a polydimethylsiloxane (PDMS) cover layer (top layer) (Fig. 2).

2.2.1. Fabrication of a bottom layer

A lotus leaf-like micropillar array was fabricated on the wall of a 40 μm deep microchannel by microfabrication techniques, including reactive ion etching (RIE). A brief process was described as follows (Fig. 3).

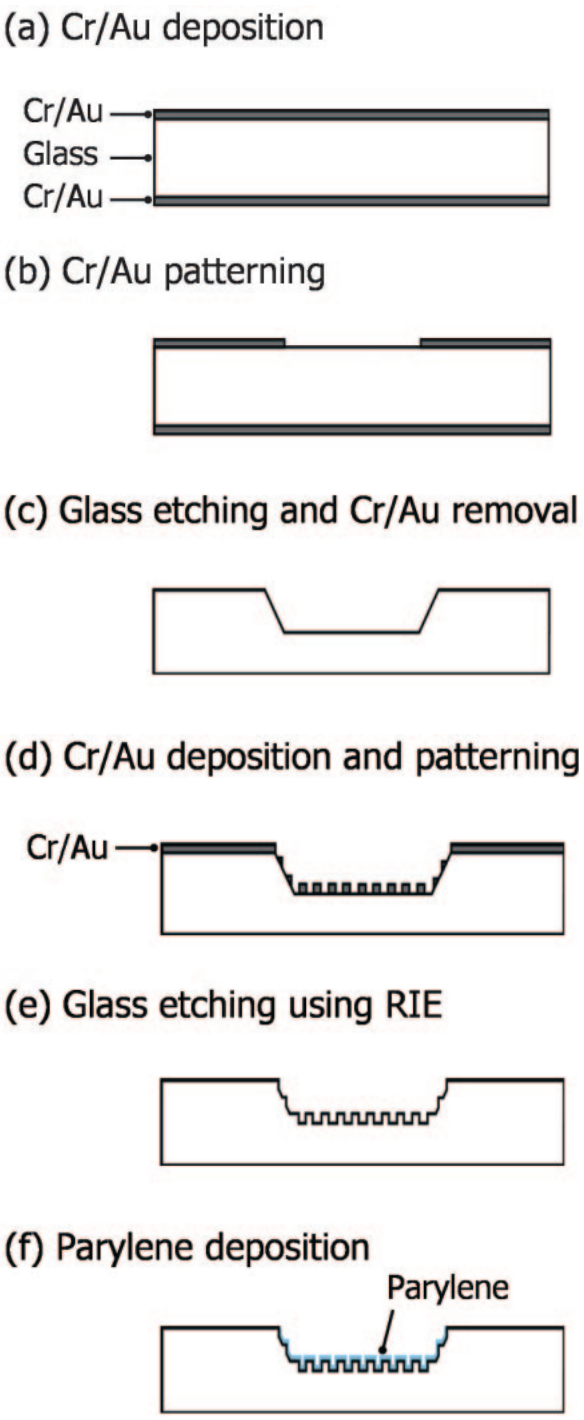

Fig. 3. Fabrication process flow for the glass substrate (bottom layer).

A) A borosilicate glass (25×25 mm, 1 mm in thickness) was first cleaned with piranha solution (7:3 H_2SO_4 : H_2O_2) for approximately 15min to remove organic impurities. The glass substrate was rinsed thoroughly with distilled water and dried with N_2. A Cr/Au (500 nm/200 nm) thin film was sputtered on both side of the glass substrate.

B) Positive resist (OFPR-800LB, 200cp) was spincoated on both side of the substrate. Then, one side of the resist film was patterned by photolithographycal manner, followed by Cr/Au-layer was wet-etched against patterned resist as a mask.

C) The glass substrate was isotropically etched by a 49 % hydrogen fluoride (HF) solution for five minutes to create a ca. 40 μm deep microchannel (Fig. 3(a)-(c)). After rinsed in distilled water, the patterned Cr/Au layer was removed by each etchant solutions.

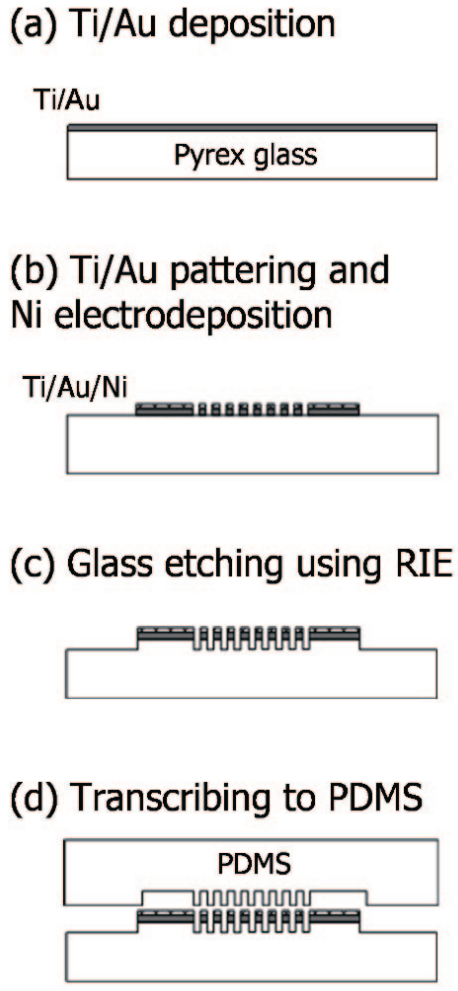

Fig. 4. Fabrication process flow for the PDMS layer (top layer).

D) The Cr/Au (1200 nm/200 nm) mask layer was recreated on the microchannel-fabricated substrate. Then negative photoresist (OMR83, 60cp) was spincoated and photolithographycally patterned, followed by Cr/Au layer was etched against patterned resist as a mask.

E) RIE was applied to construct the 20 μm height micropillar array inat the valve area of the microchannel (Fig. 3(d), (e)). The etchant gas was SF_6 (1 mTorr) and Xe (1 mTorr), and the self-bias voltage was -390 V [27]. After RIE, the substrate was washed with organic solvents and water and dried in oven for a few hours. Then oxygen plasma (130 W, 1.5 min) was applied to the substrate, and its surface was treated by silane coupling agent (3-methacryloxypropyltrimethoxy-silane, Shin-Etsu Chemical Co., Ltd).

F) Next, a 150 nm thick Parylene C film was deposited on the area of the micropillar array by a CVD method (Fig. 3(f)). CVD method enabled uniform coating of the hydrophobic Parylene C to the micro-structured hydrophilic glass substrate. Then the substrate was coated with photoresist (AZP4620), patterned and finally Parylene C film except the valve areas was etched by O_2 plasma.

G) Finally, 1 mm diameter Au electrodes were fabricated on the bottom of the microfluidic channel by standard lift-off process.

2.2.2. Fabrication of a top layer

The other component of the chip, the micropillar array-containing PDMS film (SYLPOT 184 W/C, Dow Corning Toray), was cured on a glass-made negative mold that was prepared by a similar RIE-based process (Fig.4).

A) A borosilicate glass (25×25 mm, 1 mm in thickness) was first cleaned with piranha solution (7:3 H_2SO_4 : H_2O_2) for approximately 15min to remove organic impurities. The glass was rinsed thoroughly with distilled water and dried with N_2. A Au/Ti (150 nm / 50 nm) thin film was sputtered on the glass substrate (Fig. 4 (a)).

B) Positive photoresist (PMER, P-LA900PM) was spincoated on the substrate and patterned by photolithography. The substrate was then cleaned by oxygen plasma treatment.

C) The thick nickel pattern (3000 nm) was selectively electroplated (pulse current: 20 mA, time interval: 0.1 second) on the exposed parts of the Au/Ti film (Fig. 4 (b)).

D) The mask photoresist was removed by acetone.

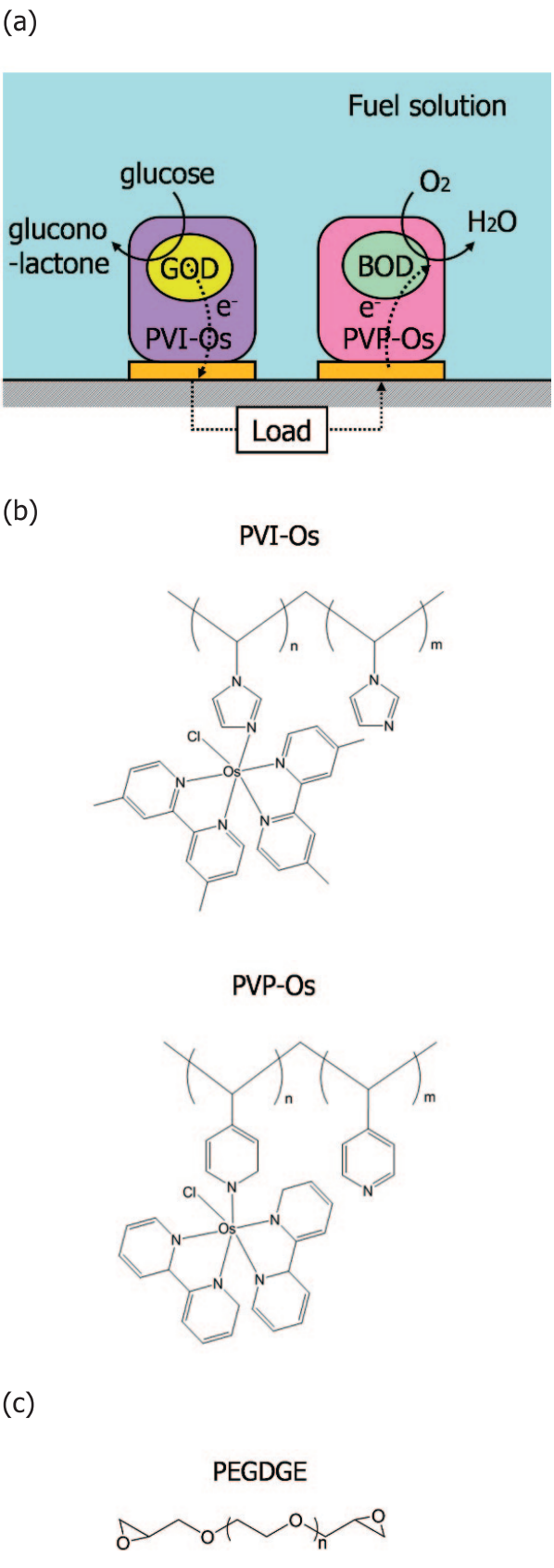

Fig. 5. (a) Structure of the electrodes, (b) chemical structures of Os-polymers and (c) chemical structure of PEGDGE.

E) The RIE was carried out using C_4F_8 (1 m Torr) and Xe (1 m Torr) as the etching gas and the self-bias voltage was set to -390 V [27] (Fig. 4 (c)). The electroplated nickel film was removed by piranha solution after RIE. After cleaning with oxygen plasma, the substrate was treated by silane coupling agent.

F) A 10:1 mixture of SYLPOT 184 W/C (Dow Corning Toray) elastomer and curing agent were poured onto the fabricated glass mold and cured at 70 °C for approximately 1.5 h. The resulting PDMS microfluidic channel was peeled off from the mold (Fig. 4 (d)).

2.3. Preparation of enzyme electrodes

The enzyme catalysts used in this paper were same as those used by Tsujimura et al [4]. Glucose oxidase (GOD) from Aspergillus niger (EC 1.1.3.4) was purchased from Wako Pure Chemical Co. Bilirubin oxidase (BOD) from Myrothecium sp. (EC 1.1.3.5) was purchased from Amano Enzyme Inc. Poly(ethylene-glycol) diglycidyl ether (PEGDGE, Mn 520) was purchased from Aldrich. Poly(1-vinylpyridine) complexed with Os(4,4'-dimethyl-2,2'-bipyridine)$_2$Cl (PVI-Os) and Poly (4-vinylpyridine) complexed with Os(2,2'-bipyridine)$_2$Cl and quaternized with bromoethyl amine (PVP-Os) were synthesized and donated by Daiichi pure chemicals Co., Ltd.

For the anode, 5 µL of PVI-Os solution (25 mg mL^{-1}), 2 µL of GOD solution (20 mg mL^{-1}) and 1.2 µL of PEGDGE solution (2.5 mg mL^{-1}) were mixed. Then, a 0.5 µL portion of the mixture was put onto an Au electrode (1 mm in diameter), and dried overnight at room temperature. Similarly, 5 µL of PVP-Os solution (25 mg mL^{-1}), 2 µL of BOD solution (20 mg mL^{-1}) and 1.2 µL of PEGDGE solution (2.5 mg mL^{-1}) were mixed and used for the cathode preparation. Here, PVP-Os is water soluble and easy to cross-link with diepoxides such as PEGDGE, which PVP-Os amines and lysyl functions of enzyme proteins. In contrast with the PVP-Os derived polymer, PVI-Os polymers are highly water soluble and do not require quaternization with bromoethylamine for easy cross-linking with water-soluble diepoxides. The cured film, though insoluble in water, is highly hydrophilic and is permeable to water-soluble ions and molecules. As shown in figure

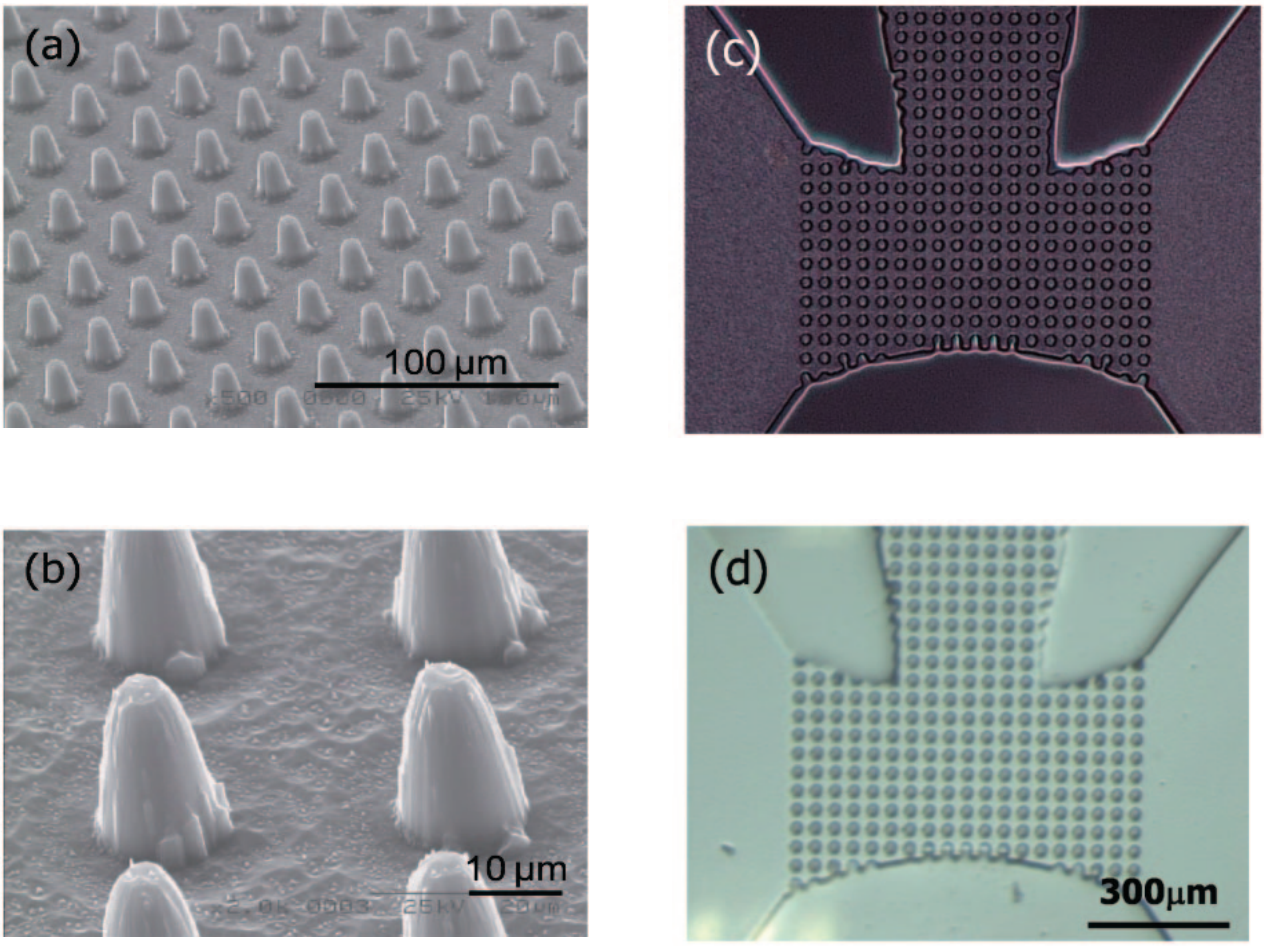

Fig. 6. (a) Low- and (b) high- magnification SEM images of the array of the 20 µm long, 15 µm diameter, 15 µm spaced micropillars and micrographs of valve areas made on a (c) PDMS and (d) glass substrate.

1, the electrocatalytic film of the anode catalyzes the electrooxidation of glucose to gluconolactone, and that of the cathode catalyzes the electroreduction of dioxigen to water. In the separator-less biofuel cell, glucose electrons reduce glucose oxidase (GOD), glucose being electro-oxidized to β-glucono-1,5-lactone. The electrons are collected and transport to the anode by an anodic redox polymer. The electrons pass then from the anode to the cathode through the external load. They are then transported from the cathode through the cathodic redox polymer to O_2-oxidized bilirubin oxidase, catalyzing its electroreduction of O_2 to water (Eq. 2). Equation (3) represents the overall cell reaction.

$$\beta\text{-D-glucose} \rightarrow \beta\text{-glucono-1,5-lactone} + 2H^+ + 2e^- \quad (1)$$

$$O_2 + 4H^+ + 4e^- \rightarrow 2H_2O \quad (2)$$

$$2\beta\text{-D-glucose} + O_2 \rightarrow 2\beta\text{-glucono-1,5-lactone} + H_2O \quad (3)$$

2.4. Measurement method

The surface hydrophobicity was evaluated by measuring the contact angle for a 1 μL water droplet. Depending on the value of the contact angle, surface properties are determined as hydrophobic (CA > 90°) or hydrophobic (CA < 90°). Surfaces with water CA higher than 150° are superhydrophobic. This very high CA is normally called apparent CA since this value does not represent the real CA value of the corresponding flat surfaces. Results are plotted as the mean value of three measurements at different places of a specimen.

The performances of the air valve were evaluated by observing the motion of solution and air at the valve areas using digital microscope (KH-3000, Hirox). A microsyringe pump (Kd Scientific, Model 210) was used to produce a steady flow in the microfluidic channel.

Electrochemical measurements were performed in 50 mM phosphate buffer solution (pH 7.0) containing 0.1 M NaCl and 0.1 M glucose at room temperature. The glucose solution was allowed to stand for at least 1 day to reach equilibrium between the α- and β-forms. The electrochemical properties of the electrodes were characterized using an Electrochemical Analyzer (Model 600S, BAS).

3. Results

3.1. Fabrication of the superhydrophobic surface

Figures 6 (a) and (b) show scanning electron microscope (SEM) images of the glass substrate etched by RIE through the patterned Cr/Au mask. These images show that we successfully fabricated a square micropillar array (20 μm long by 15 μm diameter with a 15 μm spacing). The side wall of the

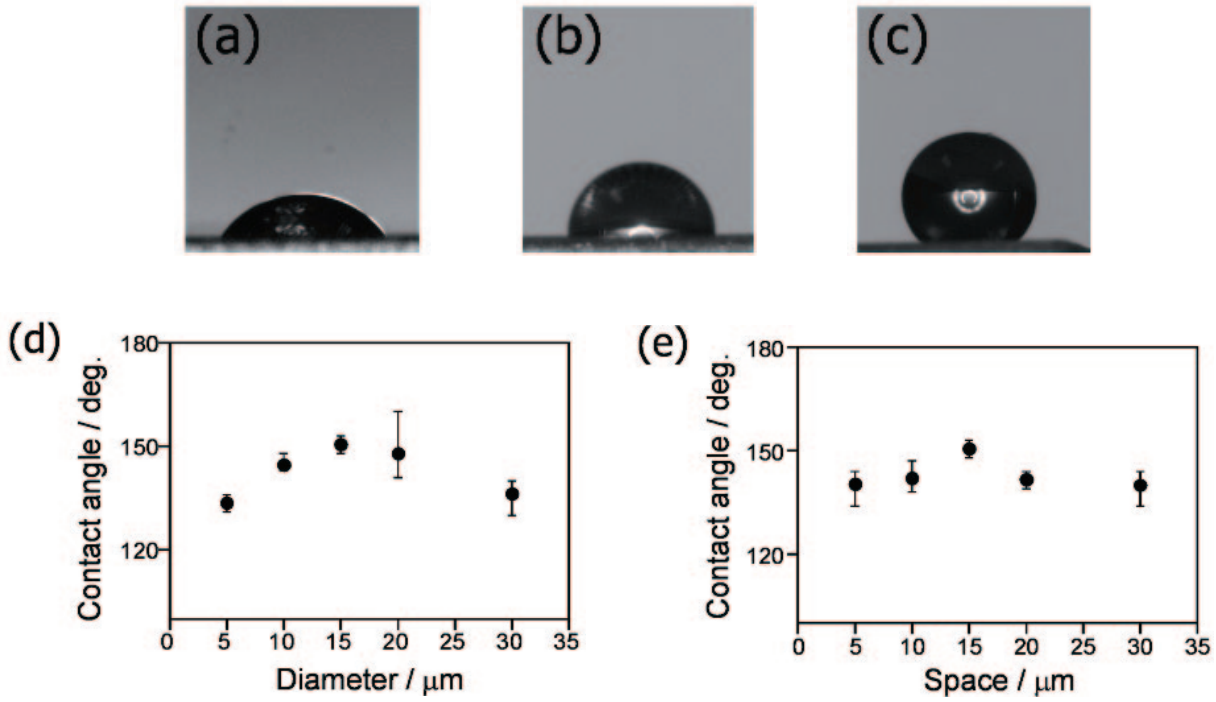

Fig. 7. Photographs of a water droplet on (a) a flat glass substrate, (b) a parylene-coated flat glass, (c) the parylene-coated micropillar array. The value of the water contact angle on the parylene-coated micropillar arrays were plotted as a function of (d) pillar diameter and (e) their spacing.

micropillars w as tapered due to the reflection of ions at the edge of the mask and/or mask erosion during the RIE process [27].

The surface hydrophobicity was evaluated by measuring the apparent contact angle (θ_c) of 1 μL water droplet. Figures 7(a)-(c) depict the images of water droplet on (a) a glass substrate, (b) a parylene-coated flat glass, and (c) the parylene-coated micropillar array. They clearly show that a micropillar structure is needed in addition to the normal hydrophobicity of the material to achieve a condition of superhydrophobic, here defined as θ_c exceeding 150°. Figures 7(d) and (e) are plots of the θ_c value as functions of diameter and spacing of the pillars; the optimum largest value of θ_c was found for pillars that were 15 μm in diameter and spaced by 15 μm.

For a chemically hydrophobic rough surface, a triphase solid-liquid-air interface form air pockets in the valleys between asperities; this contributes greatly to the increase of hydrophobicity because the θ_c of air is 180 °. In such a case, the modified Cassie-Baxter equation (equation (4)) is usually applied to estimate the apparent θ_c for water [21-26].

$$\cos\theta_c = f(1+\cos\theta) - 1 \qquad (4)$$

Here, f is the solid fraction and θ is the intrinsic contact angle on a flat surface. Equation (4) predicts that a smaller f (wider spaced, thinner pillars) exhibits a larger θ_c due to the air-trapping in a larger valley. However, practically, a surface having too small an f value cannot prevent the penetration of water into the valley, resulting in a smaller θ_c. These arguments can qualitatively explain the optimum found in Fig. 7(d) and (e). That is, the water droplet partly penetrated into the valley of micropillar array for smaller f than the optimum because the water-solid contact area was too small as compared to the size of the water droplet. Also, the cone shape of our pillars (see Fig. 6) should make water penetration easier than it would be otherwise.

The θ_c value for the micropillar array made on PDMS was systematically evaluated (data not shown) in the same way as for that made on the parylene-coated glass. The optimum design for the PDMS micropillar-array was found also to be 15μm diameter pillars separated by 15 μm, which resulted in a θ_c of ca. 170 °. It is not clear why the hydrophobicity of PDMS pillars was larger than that of the parylene-coated glass pillars as smooth surfaces of these materials had almost the same θ_c, ca. 100 °. Perhaps the mechanical properties of PDMS affects the hydrophobicity of the micropillar array in addition to the chemical and structural properties [28]. In addition, it is important to note that the contact angles for a 0.1 M glucose buffer solution were almost same as those for distilled water.

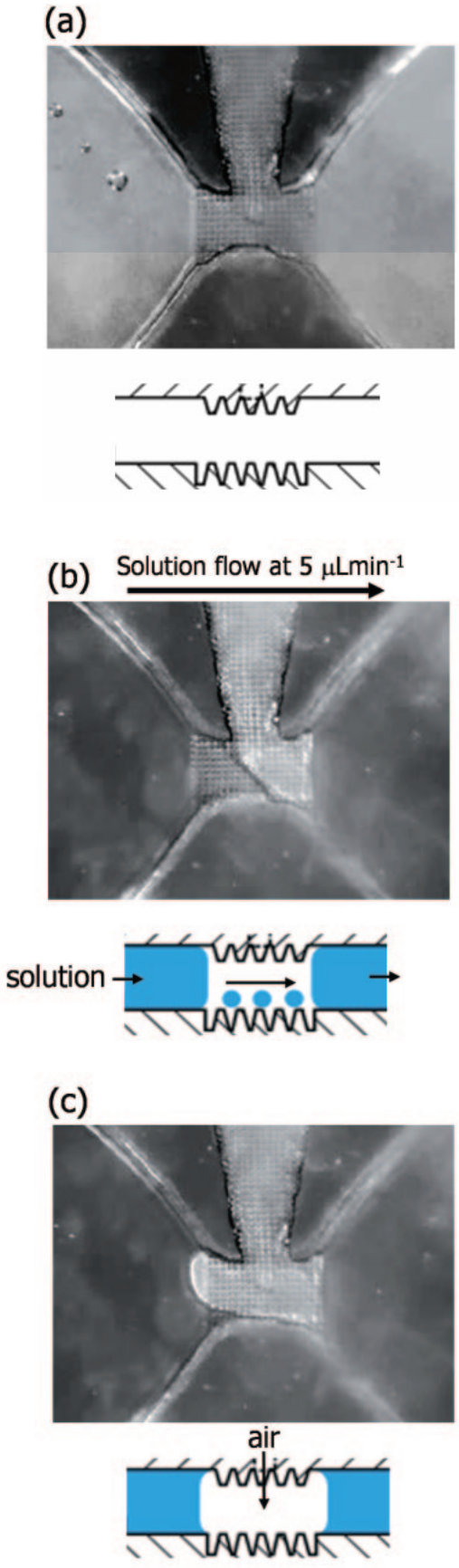

Fig. 8. Photograph of the valve area (top) and a cross-sectional illustration of the fluidic channel (bottom) before introducing solution (a), during solution flow (b), and after stopping the flow (c).

3.2. Performance of the air valves and biofuel cells

The glass layer and the PDMS layer were laminated together, and then polyethylene tubes were connected to the inlet and outlet with metal connectors, as illustrated in Fig. 2. Figure 8 shows microscopic images of the superhydrophobic gate area between cells during solution charging into a 40 μm deep channel. It is worth noting that the superhydrophobic gate was not totally wetted even while the solution is flowing (Fig. 8(b)). Such condition is possible if the solution passes through the superhydrophobic gates as small droplets or mist, as illustrated in Fig. 8(b) bottom. In this case, the cells could be ionically isolated each other. On the other hand, upon stopping solution flow (Fig. 8(c)), the cells were then clearly divided by air introduced from the air-reservoir. The air valve worked well at flow rates of 1 ~ 10 μL min^{-1}; a higher flow rate often caused an overflow of solution to the air-reservoir. The effect of channel height was also studied, and it was found that a channel that is sufficiently narrow (~ 40 μm), with a concomitantly high surface area to volume ratio, is required for effective utilization of the surface hydrophobicity so as to permit function as a valve.

Finally, the automatic series-connection of biofuel cells was attempted by utilizing the air valve system described in above. As shown in Fig. 2, the glucose/O_2 biofuel cell is composed of three sets of enzyme-modified anode/cathode pairs, each of which has a separately-measured open circuit voltage (OCV) of ca. 0.35 V, the maximum current of ca. 0.2 mA cm^{-2}, and the maximum power of ca. 0.02 mW cm^{-2} at a flow rate of 5 μL min^{-1}. The maximum currents of the present cells were smaller than the reported value [4] mainly due to the lower O_2 concentration in this study (air-saturated fuel solution) than that in the literature (O_2-saturated solution). Here, in order to prove the concept of the series-connected biofuel cells, we measured the OCV between the two ends of the circuit during fuel charging and recharging. Figure 9 shows a typical example of time plot of the OCV. At time zero, the 0.1 M glucose-containing electrolyte solution was introduced into the microchannel at 5 μL min^{-1}, and the whole channel was filled with the solution in a few minutes. The OCV was about 0.65 V under conditions of solution flow, a value roughly twice of that of a single cell. This observation indicates that one of the two gates was closed (ionically insulated) even during the solution charge. As we predicted from the picture of valve area (Fig. 8(b)), the small droplets or mist of fuel solution would transfer across the "closed" gate. The OCV quickly changed to ca. 1 V when the solution flow was stopped, suggesting that both gates were acting as closed air valves, this time providing a true series connection of the three cells. This change in OCV was reversible for successive stop and flow operations. By using a further hydrophobic material

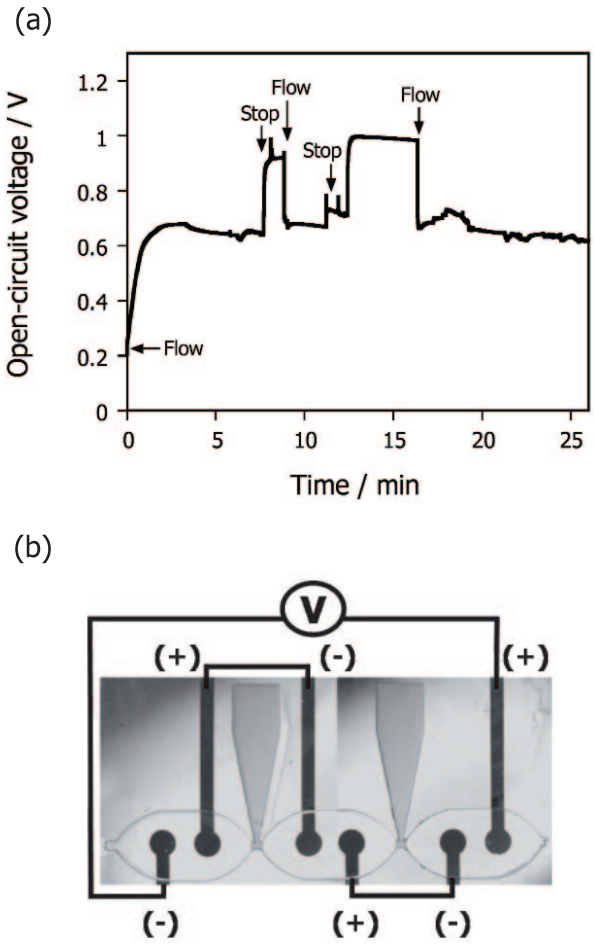

Fig. 9. (a) The time course of the open-circuit voltage (OCV) measured between the two ends of the electrode circuit during the charge and recharge of a 0.1 M NaCl and 0.1 M glucose-containing 50 mM phosphate buffer solution (pH 7). (b) A photograph of the glass substrate showing the channel, superhydrophobic gates, and three sets of anode/cathodes connected in series during the OCV measurements.

such as fluorocarbon polymers and/or by further sophisticating cell design, the stable series connection in flow will be achieved.

4. Conclusion

We demonstrated the series connection of microfluidic biofuel cells by superhydrophobic (θ_c > 150 °) gates that have an array of micropillars (20 μm high, 15 μm in diameter and with a 15 μm spacing) made by RIE-based microfabrication techniques. The superhydrophobic gates reversibly worked as air-valves for ionic isolation of each biofuel cell, resulting in the semiautomatic series connection of cells with a correspondingly increased OCV. We showed only the OCV data in this paper, since the quantitative evaluation of output current was troublesome due to gradual fuel depletion within micro-chamber in no-

flow condition. Future work will investigate the performances of advanced series-connected biofuel cells under several working conditions. In addition, although the present device is composed of a glass substrate and a PDMS film, an all-plastic series-connected biofuel cell can also be fabricated in a similar way so as to realize a flexible, freely disposable energy device. Finally, we note that the present on-chip technique for separation of solutions would be attractive also for micro-TAS devices. For example, the isolated solution pools could serve as the microwell array for ELISA measurements.

Acknowledgements

We acknowledge the support of Tohoku University Global COE Program "Global Nano-Biomedical Education and Research Network Centre".

References

[1] Heller A. Integrated medical feedback systems for drug delivery. *Aiche J* **51**, 1054-1066, 2005.
[2] Heller A. Miniature biofuel cells. *Phys Chem Chem Phys* **6**, 209-216, 2004.
[3] Barton SC, Gallaway J, and Atanassov P. Enzymatic biofuel cells for implantable and microscale devices. *Chem Rev* **104**, 4867-4886, 2004.
[4] Tsujimura S, Kano K, and Ikeda T. Glucose/O_2 biofuel cell operating at physiological conditions. *Electrochemistry* **70**, 940-942, 2002.
[5] Kamitaka Y, Tsujimura S, Setoyama N, Kajino T, and Kano K. Fructose/dioxygen biofuel cell based on direct electron transfer-type bioelectrocatalysis. *Phys Chem Chem Phys* **9**, 1793-1801, 2007.
[6] Arechederra RL, Treu BL, and Minteer SD. Development of glycerol/O_2 biofuel cell. *J Power Sources* **173**, 156-161, 2007.
[7] Moore CM, Minteer SD, and Martin RS. Microchip-based ethanol/oxygen biofuel cell. *Lab Chip* **5**, 218-225, 2005.
[8] Lim KG and Palmore GTR. Microfluidic biofuel cells: The influence of electrode diffusion layer on performance. *Biosens Bioelectron* **22**, 941-947, 2007.
[9] Palmore GTR, Bertschy H, Bergens SH, and Whitesides GM. A methanol/dioxygen biofuel cell that uses NAD^+-dependent dehydrogenases as catalysts: application of an electro-enzymatic method to regenerate nicotinamide adenine dinucleotide at low overpotentials. *J Electroanal Chem* **443**, 155-161, 1998.
[10]Gallaway J, Wheeldon I, Rincon R, Atanassov P, Banta S, and Barton SC. Oxygen-reducing enzyme cathodes produced from SLAC, a small laccase from Streptomyces coelicolor. *Biosens Bioelectron* **23**, 1229-1235, 2008.
[11]Barton SC, Sun YH, Chandra B, White S, and Hone J. Mediated enzyme electrodes with combined micro- and nanoscale supports. *Electrochem Solid State Lett* **10**, B96-B100, 2007.
[12]Tominaga M, Otani M, Kishikawa M, and Taniguchi I. UV-ozone treatments improved carbon black surface for direct electron-transfer reactions with bilirubin oxidase under aerobic conditions. *Chem Lett* **35**, 1174-1175, 2006.
[13]Kakehi N, Yamazaki T, Tsugawa W, and Sode K. A novel wireless glucose sensor employing direct electron transfer principle based enzyme fuel cell. *Biosens Bioelectron* **22**, 2250-2255, 2007.
[14]Tamaki T and Yamaguchi T. High-surface-area three-dimensional biofuel cell electrode using redox-polymer-grafted carbon. *Ind Eng Chem Res* **45**, 3050-3058, 2006.
[15]Sato F, Togo M, Islam MK, Matsue T, Kosuge J, Fukasaku N, Kurosawa S, and Nishizawa M. Enzyme-based glucose fuel cell using Vitamin K_3-immobilized polymer as an electron mediator. *Electrochem Commun* **7**, 643-647, 2005.
[16]Togo M, Takamura A, Asai T, Kaji H and Nishizawa M. An enzyme-based microfluidic biofuel cell using vitamin K_3-mediated glucose oxidation. *Electrochim. Acta* **52**, 4669-4674, 2007.
[17]Togo M, Takamura A, Asai T, Kaji H, and Nishizawa M. Structural studies of enzyme-based microfluidic biofuel cells. *J Power Sources* **178**, 53-58, 2008.
[18]Furukawa Y, Moriuchi T, and Morishima K. Design principle and prototyping of a direct photosynthetic/metabolic biofuel cell (DPMFC). *J Micromech Microeng* **16**, S220-S225, 2006.
[19]Chiao M, Lam KB, and Lin LW. Micromachined microbial and photosynthetic fuel cells. *J Micromech Microeng* **16**, 2547-2553, 2006.
[20]Wenzel RN. Resistance of solid surfaces to wetting by water. *Ind Eng Chem* **28**, 988-994, 1936.
[21]Li XM, Reinhoudt D, and Crego-Calama M. What do we need for a superhydrophobic surface? A review on the recent progress in the preparation of superhydrophobic surfaces. *Chem Soc Rev* **36**, 1350-1368, 2007.
[22]Hosono E, Fujihara S, Honma I, and Zhou HS. Superhydrophobic perpendicular nanopin film by the bottom-up process. *J Am Chem Soc* **127**, 13458-13459, 2005.
[23]Zhang L, Zhou ZL, Cheng B, DeSimone JM, and Samulski ET. Superhydrophobic behavior of a perfluoropolyether lotus-leaf-like topography. *Langmuir* **22**, 8576-8580, 2006.
[24]Feng XJ and Jiang L. Design and creation of superwetting/antiwetting surfaces. *Adv Mater* **18**, 3063-3078, 2006.
[25]Sun M, Luo C, Xu L, Ji H, Ouyang Q, Yu D, and Chen Y. Artificial Lotus Leaf by Nanocasting. *Langmuir* **21**, 8978-8981, 2005.
[26]Cassie ABD and Baxter S. Wettability of porous surfaces. *Trans Faraday Soc* **40**, 0546-0550, 1944.
[27]Li XH, Abe T, and Esashi M. Deep reactive ion etching of Pyrex glass using SF_6 plasma. *Sens Actuator A-Phys* **87**, 139-145, 2001.
[28]Extrand CW and Kumagai Y. Contact Angles and Hysteresis on Soft Surfaces. *Journal of Colloid and Interface Science* **184**, 191-200, 1996.